Research Article

Stagnation Point Heat Flow and Mass Transfer in a Casson Nanofluid with Viscous Dissipation and Inclined Magnetic Field

Wasiu Toyin Akaje[a*], **Olajuwon B. I**[b]

Department of Mathematics, Federal University of Agriculture, Abeokuta, Nigeria
E-mail: [a]akajewasiu@gmail.com, [b]ishola1@gmail.com

Access this article online		
Received on: November 6, 2020	**Accepted on:** Janaury 7, 2021	**Published on:** June 30, 2021
DOI: 10.25079/ukhjse.v5n1y2021.pp38-49	**E-ISSN:** 2520-7792	

Copyright © 2021 Akaje&Olajuwon. This is an open access article with Creative Commons Attribution Non-Commercial No Derivatives License 4.0 (CC BY-NC-ND 4.0)

Abstract

Influence of slip and inclined magnetic field on stagnation-point flow with chemical reaction are studied. Implementation of the similarity transformations, transformed the fluid non-linear ordinary differential equations and numerical computation is performed to solve those equations using Spectral Collocation Method. Various pertinent parameters on fluid flow, temperature and concentration distributions of the Casson nanofluid flow as well as the local skin friction coefficient, local Nusselt number, and Sherwood number are graphically displayed. The results indicate that thermophoresis parameter N_t enhanced the temperature and nanoparticle concentration profiles, because a rise in thermophoresis parameter enhances the thermophoresis force within the flow regime. Values of both local Nusselt and Sherwood numbers are enhanced with an increase in Hartman number (magnetic field parameter). The present results are compared with previously reported ones and are found to be in excellent agreement.

Keywords: Magnetic Field, Casson Nanofluid, Stagnation Point, Viscous dissipation.

1. Introduction

The growing attention of many researchers recently on flow and heat transfer of a viscous and incompressible fluid flowing through an elongating surface is because of its numerous engineering applications, especially in industry and manufacturing processes. For example, glass fibre production, paper production, extrusion of polymers, refrigeration, cooling of electronic equipment, copper wires drawing, and crude oil purification. To obtain the production quality for such processes, the heat transfer, and the flow field are highly needed. Various researchers recently are engaged in using the non-Newtonian heat transfer characteristics flowing through a stretching sheet. In 1970, Crane was the first author to work on the flow of fluid over a stretching sheet with linear order. In the work, the steady-state similarity solution was obtained. Mahapatra & Gupta in 2001 studied an incompressible viscous electrically conducting fluid past a stretching sheet. The influence of variable thermal conductivity and heat source on MHD boundary layer flow of electrically conducting fluid is investigated by (Alsedais, 2017). It was found that at A = 2.0 the skin-friction at the surface increases and decreases at A = 2.0 with an increase in the Casson parameter. Zaimi & Ishak in 2016 reported the slip effects on stagnation-point flow through a stretching vertical sheet.

Pavlov in 1974 considered the influence of the external magnetic field in the hydromagnetic flow over a stretching sheet. Bhattacharyya & Layek in 2010 investigated the effect of suction/blowing on hydromagnetic boundary layer flow over a permeable stretching sheet.

The influence of chemical reaction on slip flow of magnetohydrodynamic heat and mass Casson fluid over a stretching sheet is analyzed by Kumar & Gangadhar in 2015 and it was observed that the reduction of some parameters such as magnetic and momentum slip reduce the fluid flow. Rao & Sreenadh in 2017 studied the exponentially inclined

permeable flow of a Casson fluid. The result shows that temperature distribution reduces as Prandtl number, thermal slip factor, suction parameter increase and enhances with radiation parameter, Eckert number, and Magnetic parameter. Soid and Ishak et al. in 2009 studied MHD stagnation point flow over a stretching/shrinking sheet (Fang et al., 2009)obtained the exact solution on the magnetohydrodynamic flow and mass transfer with slip condition through a stretching sheet.

Nanofluids are gaining more attention from many researchers today because of its significant applications of enhancing fluid transfer performance properties, particularly concerning heat transfer Choi & Eastman in 1995 were the first author to introduce the concept of Nanofluid where he proposed the suspension of nanoparticles. The suspension of particles such as metals, metals oxides, carbides, nitrides, carbon, and nanotubes are dispersed in a continuous medium (base fluids) such as water, ethylene, glycol, and engine oil of size less than 100nm is known as Nanofluids. After Choi, many authors worked on Nanofluids and Casson Nanofluids. Meraj & Junaid in 2015 studied hydromagnetic Casson nanofluid through a non-linearly stretching sheet, it was reported that Brownian motion does not have an impact on fluid temperature and heat transfer rate from the sheet while both temperature and nanoparticle volume fraction are decreasing functions of thermophoresis parameters. The hydromagnetic chemically reactive nanofluid flow past a permeable flat plate in a porous medium was investigated by Reddy et al. in 2016. Analytic and numeric solutions were examined by Awais et al. in 2015. It was observed that a rise in the magnetic field parameter results in a decrease in fluid particles inter-molecular movement which leads to an enhancement of fluid temperature. Also, the presence of a heat source in a system can enhance the temperature whereas a heat sink causes a decrease in temperature. The hydromagnetic and heat transfer flow of Williamson nanofluid through a stretching sheet with variable thickness and the variable thermal conductivity were presented in Reddy et al. in 2017. Nageeb et al. studied the unsteady free convective hydromagnetic chemically reactive boundary-layer flow of nanofluid over-stretching surfaces using the spectral relaxation method (Haroun et al., 2015). Mohamed and Afify investigated chemically reactive Casson Nanofluid flow through stretching sheet with slip boundary condition, viscous dissipation in (Afify, 2017).

In this paper, the work of Afify (Haroun et al., 2015) is extended by including stagnation point, heat generation, and the effect of inclined magnetic field on the problem of the steady Casson nanofluid flowing over a stretching sheet.

2. Mathematical Analysis

We analyzed the steady two-dimensional incompressible flow of electrically conducting and chemically reactive Casson nanofluid bounded by a stretching sheet at $y = 0$, with the flow being confined in $y > 0$. $u_w = bx$ is the stretched linear velocity where b is the positive constant. The strength of the inclined magnetic field is B_o, and here $T_\infty and\ C_\infty$ are the ambient temperature and nanoparticle concentration fields with $T_\infty > T_w$. Thermophoresis and Brownian motion of nanoparticles are taken into consideration. The rheological equation of state of an isotropic and incompressible flow of Casson fluid is given by (Haroun et al., 2015):

$$\tau_{ij} = \begin{cases} \left(\mu_B + \frac{p_y}{\sqrt{2\pi}}\right) 2e_{ij}, & \pi > \pi_c \\ \left(\mu_B + \frac{p_y}{\sqrt{2\pi_c}}\right) 2e_{ij}, & \pi < \pi_c \end{cases} \tag{1}$$

where μ_D is the plastic dynamic viscosity of the non-Newtonian fluid, p_y is the yield stress of fluid, π is the product of the component of deformation rate with itself, namely, $\pi = e_{ij}e_{ij}, e_{ij}$ is the $(i,j)^{th}$component of the deformation rate and π_c is the critical value of π based on the non-Newtonian model. The governing equations of momentum, energy, and mass are:

$$\frac{\partial u}{\partial x} + \frac{\partial v}{\partial y} = 0 \tag{2}$$

$$u\frac{\partial u}{\partial x} + v\frac{\partial u}{\partial y} = U\frac{dU}{dx} + v\left(1 + \frac{1}{\beta}\right)\frac{\partial^2 u}{\partial y^2} + \frac{\sigma B_o^2}{\rho}(U-u)\sin^2\varphi \tag{3}$$

$$u\frac{\partial T}{\partial x} + v\frac{\partial T}{\partial y} = \frac{k}{\rho C_p}\frac{\partial^2 T}{\partial y^2} + \tau\left[D_B\left(\frac{\partial C}{\partial y}\frac{\partial T}{\partial y}\right) + \frac{D_T}{T_\infty}\left(\frac{\partial T}{\partial y}\right)^2\right] + \frac{\mu}{\rho C_p}\left(1 + \frac{1}{\beta}\right)\left(\frac{\partial u}{\partial y}\right)^2 + \frac{\sigma B_o^2}{\rho C_p}(U-u)^2\sin^2\varphi \tag{4}$$

$$u\frac{\partial C}{\partial x}+v\frac{\partial C}{\partial y}=D_B\frac{\partial^2 C}{\partial y^2}+\frac{D_T}{T_\infty}\frac{\partial^2 T}{\partial y^2}-K_o(C-C_\infty) \tag{5}$$

With the given boundary conditions:

$$u=u_w+\left(1+\frac{1}{\beta}\right)N\,\rho v\frac{\partial u}{\partial y},$$

$$v=0, T=T_w+K_1\frac{\partial T}{\partial y},\ \ C=C_w+K_2\frac{\partial C}{\partial y},\qquad at\ \ y=0,$$

$$u=0,\qquad T=T_\infty,\qquad C=C_\infty,\quad as\quad y\to\infty \tag{6}$$

In this work, the induced magnetic field is ignored. Consider the following dimensionless transformations

$$\eta=\left(\frac{b}{\upsilon}\right)^{\frac{1}{2}}y,\ \ \psi(x,y)=(b\upsilon)^{\frac{1}{2}}xf(\eta),\quad \theta(\eta)=\frac{T-T_\infty}{T_w-T_\infty},\ \ \phi(\eta)=\frac{C-C_\infty}{C_w-C_\infty} \tag{7}$$

Using the stream function $\psi(x,y)$ such that

$$u=\frac{\partial\psi}{\partial y},\ \ v=-\frac{\partial\psi}{\partial x} \tag{8}$$

Therefore the equation (2) is satisfied. From the given transformations mentioned above, 3 to 6 become

$$\left(1+\frac{1}{\beta}\right)f'''(\eta)+f(\eta)f''(\eta)-\left(f'(\eta)\right)^2+H_a\left(A-f'(\eta)\right)\sin^2\varphi+A^2=0 \tag{9}$$

$$\frac{1}{Pr}\theta''(\eta)+f\theta'(\eta)+N_t\phi'(\eta)\theta'(\eta)+N_t(\theta'(\eta))^2+\left(1+\frac{1}{\beta}\right)E_c\left(f''(\eta)\right)^2$$

$$+H_aE_c\left(A-f'(\eta)\right)^2\sin^2\varphi+Q\theta(\eta)=0 \tag{10}$$

$$\phi''(\eta)+\mathrm{Le}f\phi'(\eta)+\frac{N_t}{N_b}\theta''(\eta)-Le\chi\phi(\eta)=0 \tag{11}$$

$$f(0)=0,\qquad f'(0)=1+\lambda\left(1+\frac{1}{\beta}\right)f''(0),$$

$$\theta(0)=1+\gamma\theta'(0),\quad \phi(0)=1+\delta\phi'(0)$$

$$f'(\infty)=0,\ \theta(\infty)=0,\ \phi(\infty)=0 \tag{12}$$

Here prime represents differentiation with respect to η. The flow parameters are defined as below:

$$Pr=\frac{v}{\alpha},\qquad Le=\frac{v}{D_B},\qquad \lambda=N\rho(vb)^{\frac{1}{2}},\qquad \gamma=K_1\left(\frac{b}{v}\right)^{\frac{1}{2}},\qquad \chi=\frac{K_o}{b},$$

$$E_c=\frac{{u^2}_w}{c_p(T_w-T_\infty)},\qquad \delta=K_2\left(\frac{b}{v}\right)^{\frac{1}{2}},\qquad N_b=\frac{(\rho c)_pD_B(C_w-C_\infty)}{(\rho c)_f v},$$

$$N_t=\frac{(\rho c)_pD_T(T_w-T_\infty)}{(\rho c)_f vT_\infty},\quad H_a=\frac{\sigma {B_o}^2}{\rho b} \tag{13}$$

The physical quantities of engineering interest are the Skin friction coefficient (rate of shear stress), the Nusselt number (rate of heat transfer), and the Sherwood number (rate of mass transfer).

The local Skin-friction Cf_x, local Nusselt Number Nu_x, and local Sherwood Number Sh_x which are defined as

$$Cf_x=\frac{\tau_w}{\rho{u^2}_w},\qquad Nu_x=\frac{xq_w}{k(T_w-T_\infty)},\qquad Sh_x=\frac{xq_m}{D_B(C_w-C_\infty)} \tag{14}$$

$$\tau_w=\left(\mu_B+\frac{p_y}{\sqrt{2\pi_c}}\right)\left(\frac{\partial u}{\partial y}\right)_{y=0},q_w=-k\left(\frac{\partial T}{\partial y}\right)_{y=0},q_m=\ -D_B\left(\frac{\partial C}{\partial y}\right)_{y=0} \tag{15}$$

In terms of dimensionless quantities (14) we have

$$Re_x^{1/2} C_f = \left(1 + \frac{1}{\beta}\right) f''(0), \qquad \frac{N_u}{Re_x^{1/2}} = -\theta'(0) \quad , \frac{Sh_x}{Re_x^{1/2}} = -\phi'(0), \tag{16}$$

where $Re_x = \frac{x u_w}{v}$ is the local Reynolds number.

3. Numerical Solution

The systems of nonlinear differential equations (9-11) parallel to the boundary conditions (12) are solved numerically using the Chebyshev spectral collocation method. In this method, the unknown functions, $f(\eta), \theta(\eta) and\ \phi(\eta)$ is approximated by the sum of the basic functions $T_n(\eta)$ (Shen et al., 2011; Sun et al., 2012).

$$f(\eta) = \sum_{n=o}^{N} a_n T_n(\eta) \tag{17}$$

$$\theta(\xi) = \sum_{n=0}^{N} b_n T_n(\eta) \tag{18}$$

$$\phi(\eta) = \sum_{n=0}^{N} c_n T_n(\eta) \tag{19}$$

The basic functions are taken as the Chebyshev polynomials, in (17), (18), and (19) which defined in the interval $-1 \leq \eta \leq 1$ as

$$T_n(\eta) = \cos(N \cos^{-1} \eta) \tag{20}$$

$a_n, b_n and\ c_n$ are unknown constant to be obtained. $[o, \infty]$ is the considered flow problem domain, which transformed into the $[-1,1]$ of the definition of basis functions, by using the below transformation

$$\eta = \frac{2p}{p_\infty - 1} \tag{21}$$

where η_∞ denotes the edge of the boundary layer, by substituting (17), (18), and (19) into (9-11), non-zero residuals were obtained. The coefficient a_n,b_n and c_n were chosen in such a way that the obtained residues were minimized throughout the domain.

Table 1 shows the Comparison of results for $-\theta'(0)$ and $-\emptyset'(0)$ with N_t, N_b λ and E_c for β = 0.5, λ = y = δ = 0.2, Pr = 4, Le = 5 and A = Q = H = 0.

Table 1. shows the Comparison of results for 〖-θ〗^' (0) and 〖-∅〗^' (0) with Nt, Nb λ and Ec for β = 0.5, λ = y = δ = 0.2, Pr = 4, Le = 5 and A = Q = H = 0.

N_t	N_b	λ	Ec	Ahmed and Afify $-\theta'(0)$[16]	Present results $-\theta'(0)$	Ahmed and Afify $-\emptyset'(0)$ (Haroun et al., 2015)	Present results $-\emptyset'(0)$
0.1	0.1	0.2	0.2	0.655854	0.654296	1.19213	1.19232
0.3	0.1	0.2	0.2	0.510010	0.508726	1.22598	1.22667
0.5	0.1	0.2	0.2	0.394448	0.393369	1.45703	1.45778
0.1	**0.2**	0.2	0.2	0.550359	0.551452	1.27665	1.27465
0.1	**0.4**	0.2	0.2	0.371446	0.371348	1.31245	1.30315
0.1	**0.6**	0.2	0.2	0.235575	0.235684	1.31891	1.31663
0.1	0.1	**- 0.2**	0.2	0.664530	0.66554	0.637467	0.636539
0.1	0.1	**0.0**	0.2	0.659002	0.658105	0.961861	0.960761
0.1	0.1	**0.4**	0.2	0.654009	0.653702	1.367830	1.366820
0.1	0.1	0.2	**0.0**	0.795783	0.794862	1.113521	1.112604
0.1	0.1	0.2	**1.0**	0.082093	0.083140	1.515737	1.516703
0.1	0.1	0.2	**1.3**	- 0.139103	- 0.138211	1.641030	1.640031

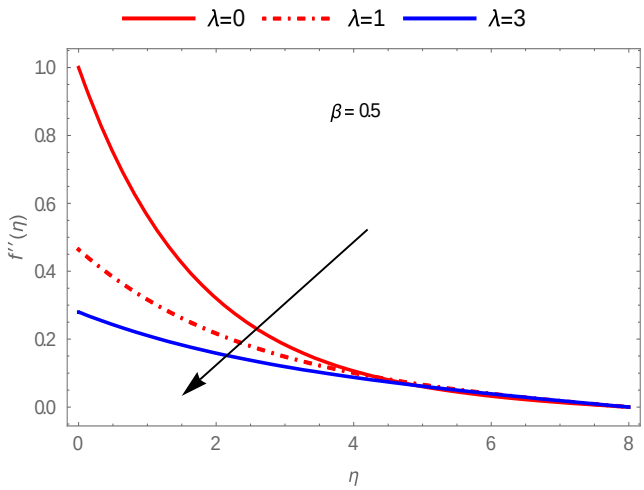

Figure 1. Effect of λ on $f''(\eta)$.

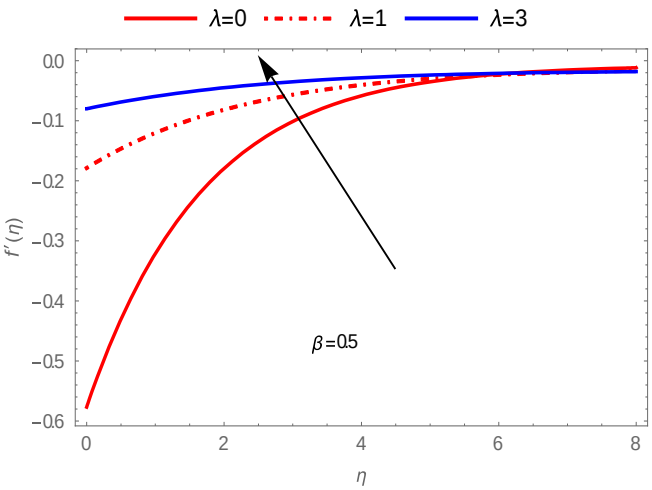

Figure 2. Effect of λ on $f'(\eta)$.

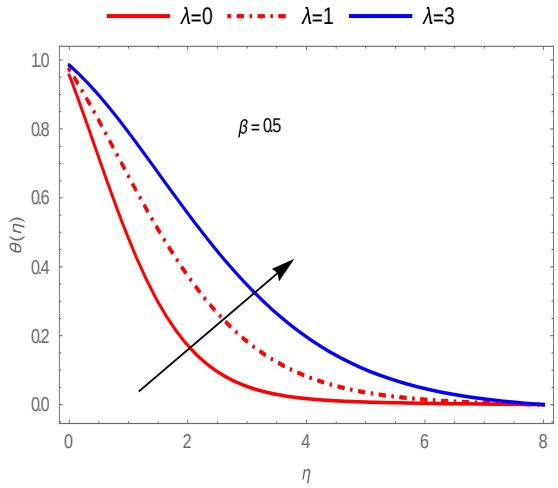

Figure 3. Effect of λ on $\theta(\eta)$.

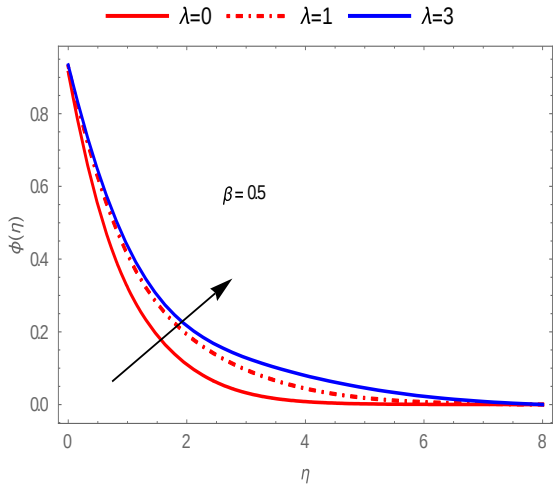

Figure 4. Effect of λ on $\phi(\eta)$.

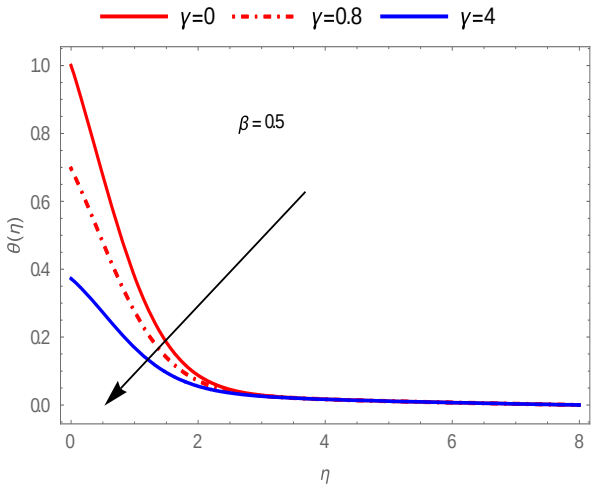

Figure 5. Effect of γ on $\theta(\eta)$.

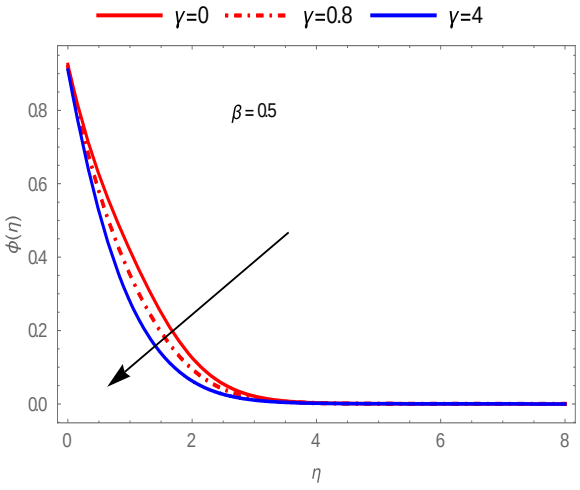

Figure 6. Effect of γ on $\phi(\eta)$.

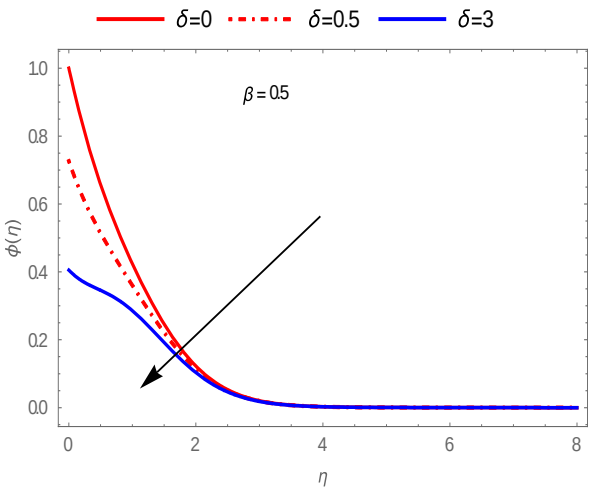

Figure 7. Effect of δ on $\theta(\eta)$.

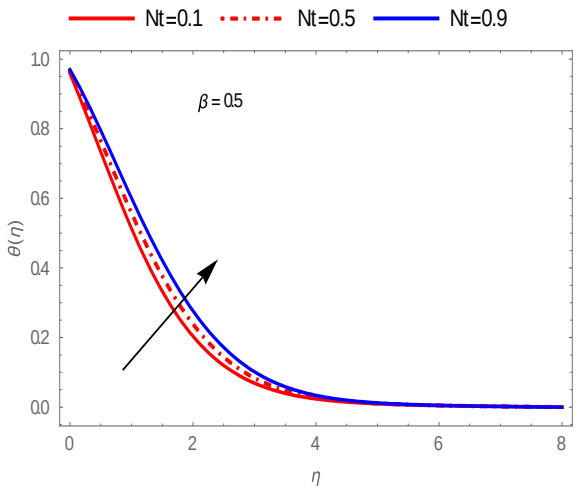

Figure 8. Effect of N_t on $\theta(\eta)$.

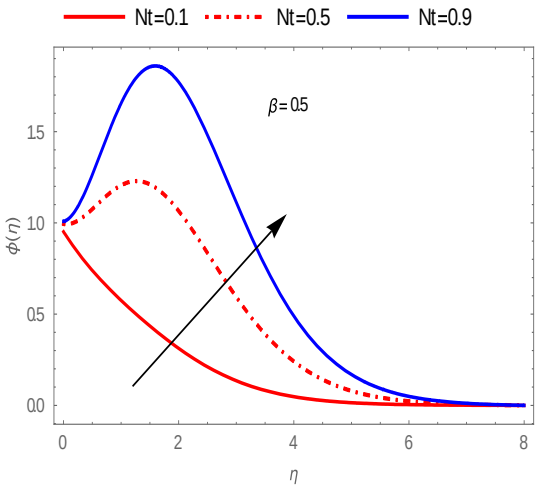

Figure 9. Effect of $N_t on\ \phi(\eta)$.

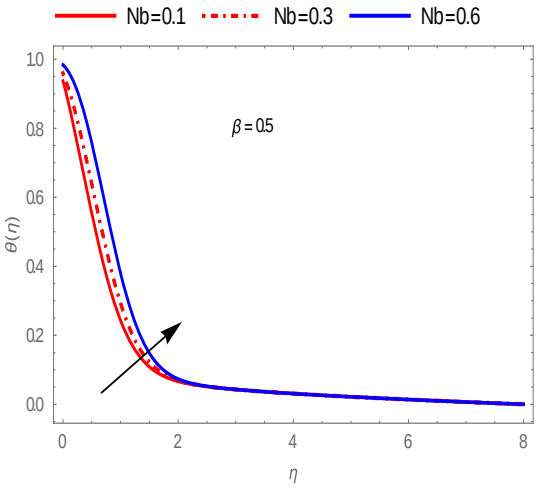

Figure 10. Effect of N_b on $\theta(\eta)$.

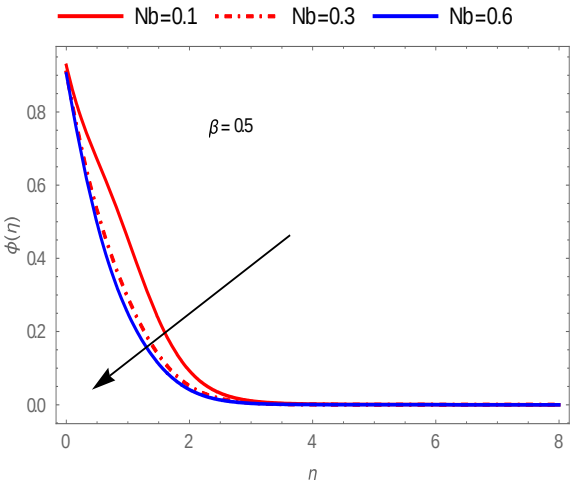

F igure 11. Effect of N_b on $\phi(\eta)$.

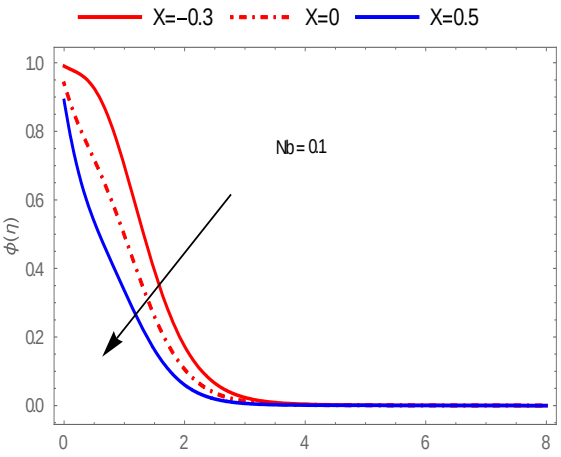

Figure 12. Effect of X on $\phi(\eta)$ for $N_b = 0.1$.

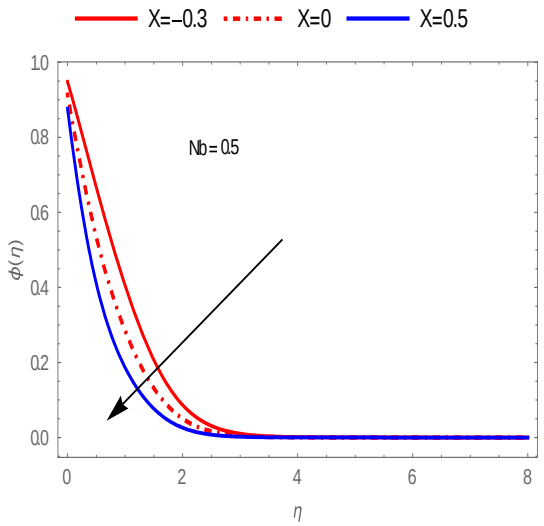

Figure 13. Effect of X on $\phi(\eta)$ for $Nb = 0.5$.

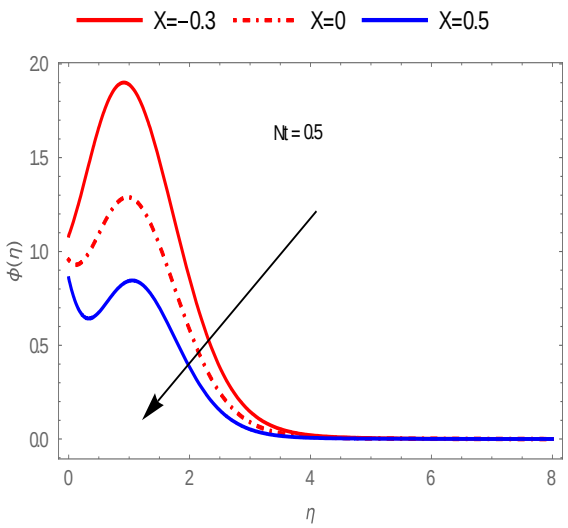

Figure 14. Effect of X on $\phi(\eta)$ for $Nt = 0.5$.

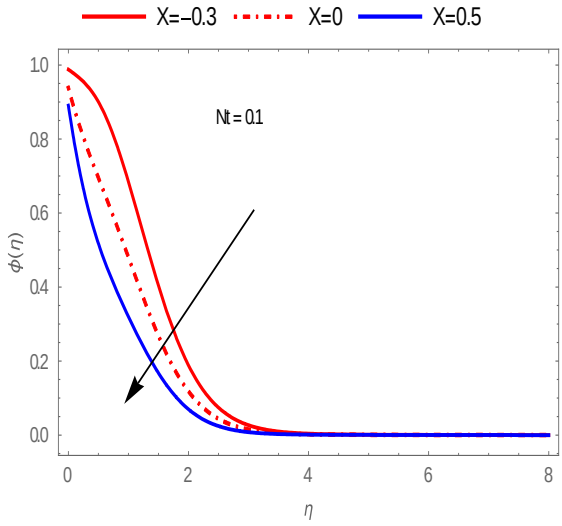

Figure 15. Effect of X on $\phi(\eta)$ for $N_t = 0.1$.

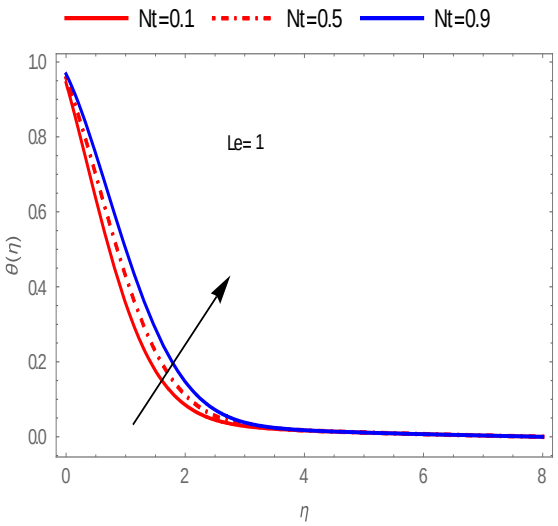

Figure 16. Effect of N_t on $\theta(\eta)$ for $Le = 1$.

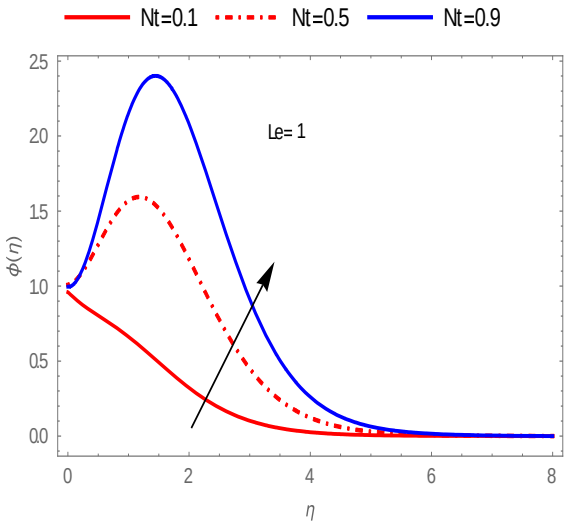

Figure 17. Effect of N_t on $\phi(\eta)$ for $Le = 1$.

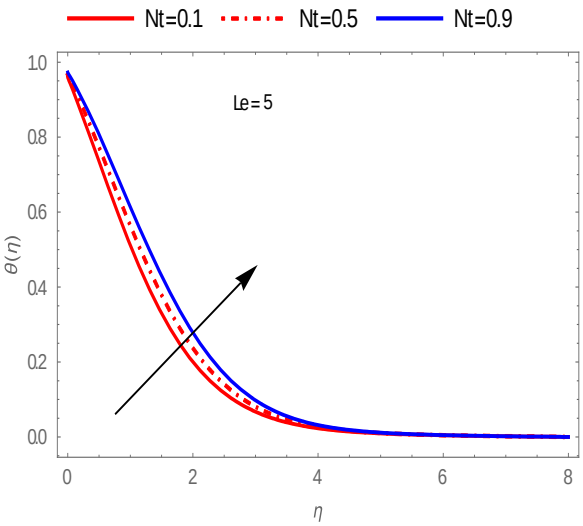

Figure 18. Effect of N_t on $\theta(\eta)$ for $Le = 5$.

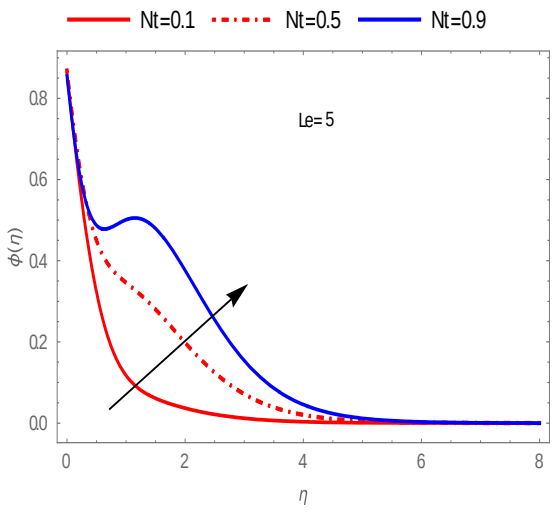

Figure 19. Effect of N_t on $\phi(\eta) for$ $Le = 5$.

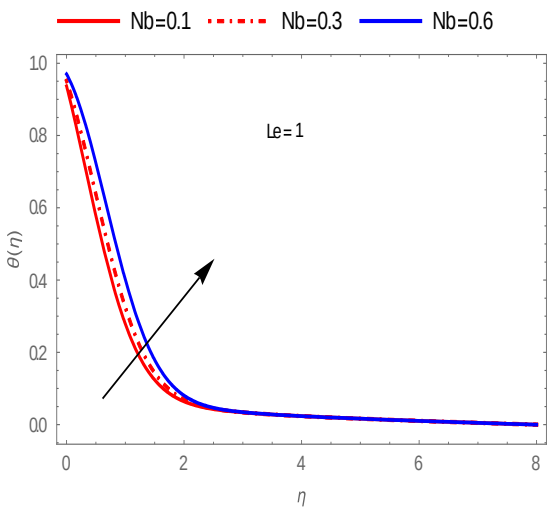

Figure 20. Effect of N_b on $\theta(\eta)$ for $Le = 1$.

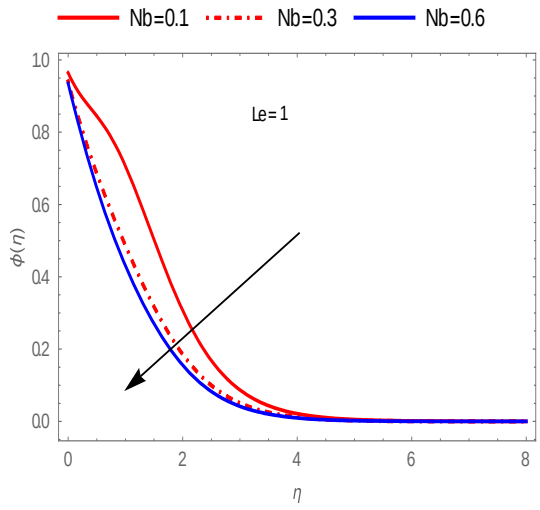

Figure 21. Effect of Nb on $\theta(\eta) for$ $Le = 1$.

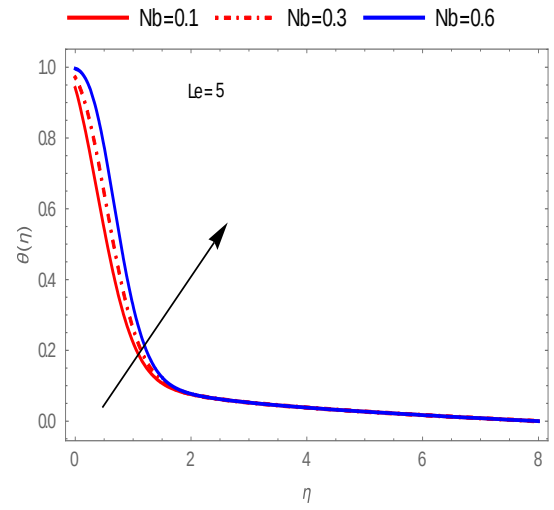

Figure 22. Effect of Nb on $\theta(\eta)$ for $Le = 5$.

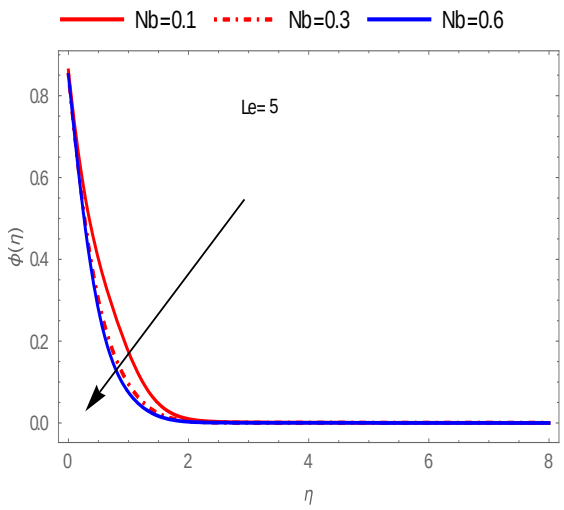

Figure 23. Effect of N_b on $\phi(\eta) for$ $Nb = 5$.

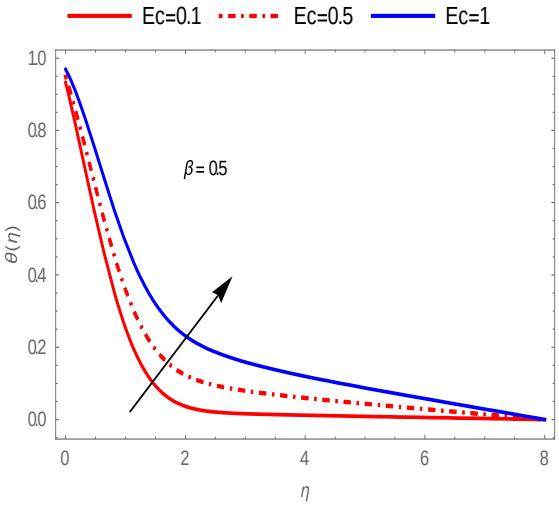

Figure 24. Effect of E_c on $\theta(\eta)$.

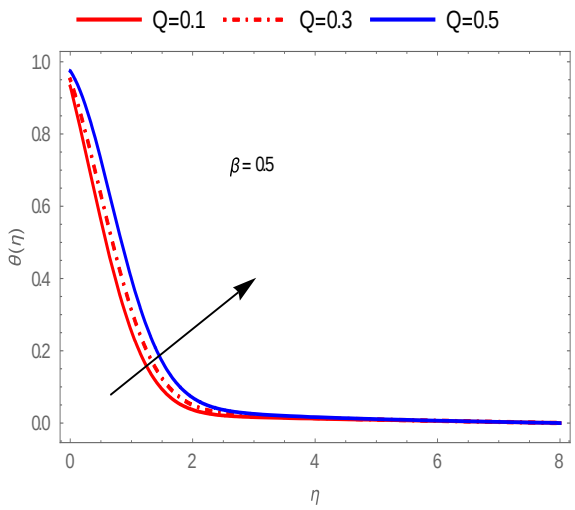

Figure 25. Effect of Q on $\theta(\eta)$.

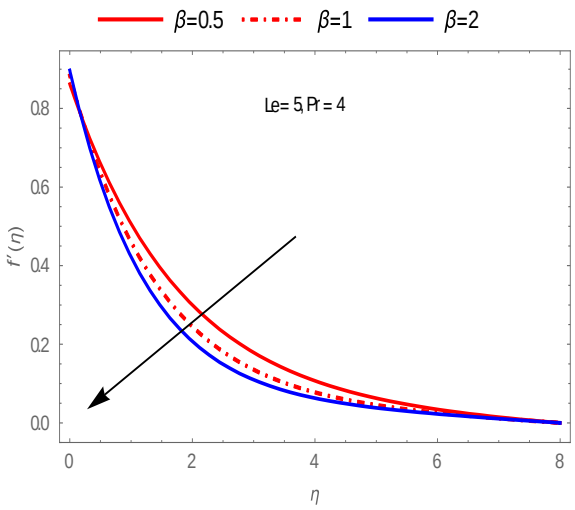

Figure 26. Effect of β on $f'^{(\eta)}$.

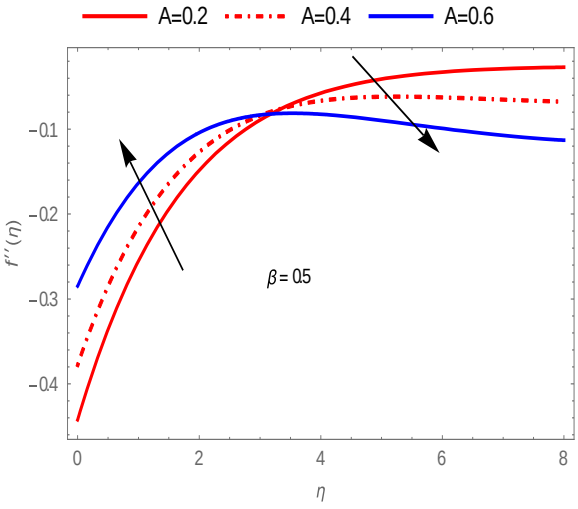

Figure 27. Effect of A on $f''(\eta)$.

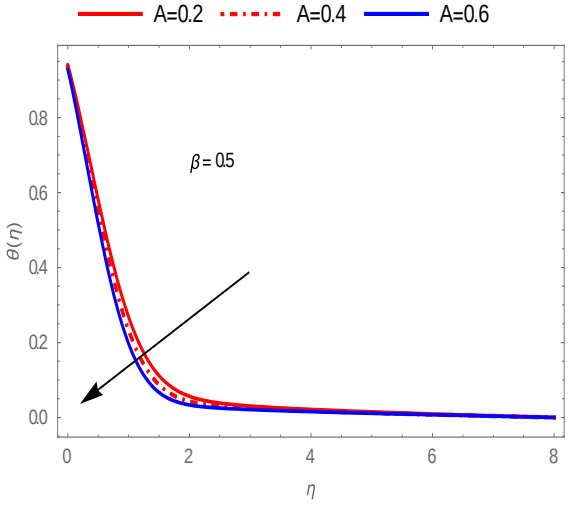

Figure 28. Effect of A on f′(η).

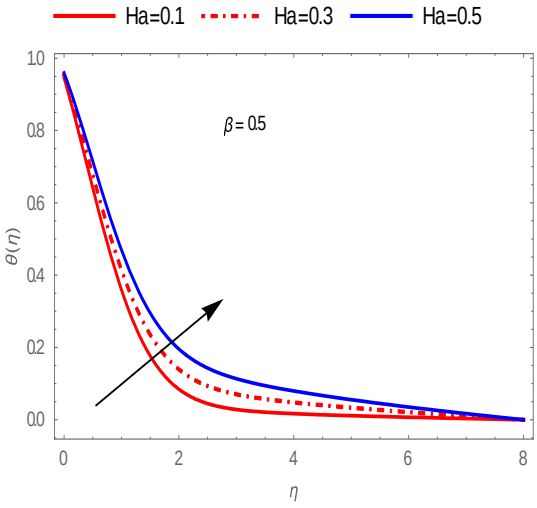

Figure 29. Effect of Ha on $\theta(\eta) for$ $\beta = 0.5$.

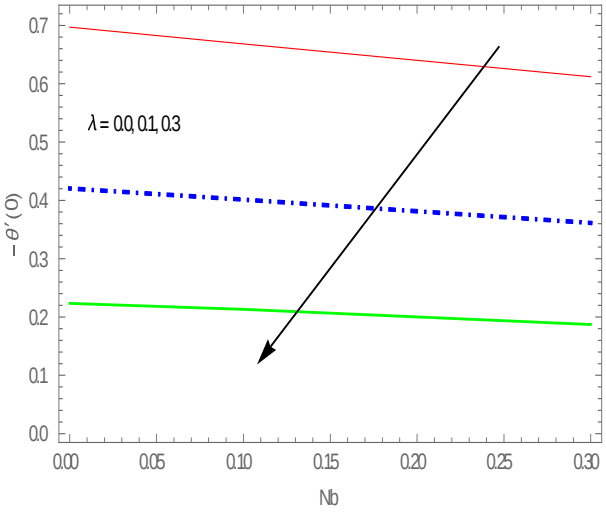

Figure 30. Effect of N_b and λ-θ(η).

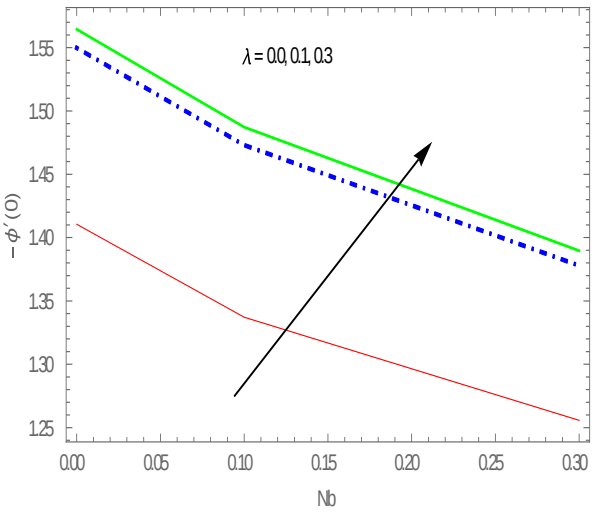

Figure 31. Effect of $N_b and\ \lambda - \phi'(\eta)$.

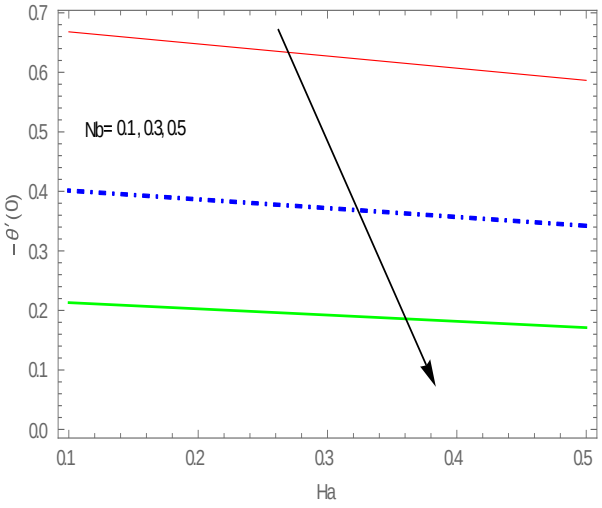

Figure 32. Effect of N_b and $H_a - \theta(\eta)$.

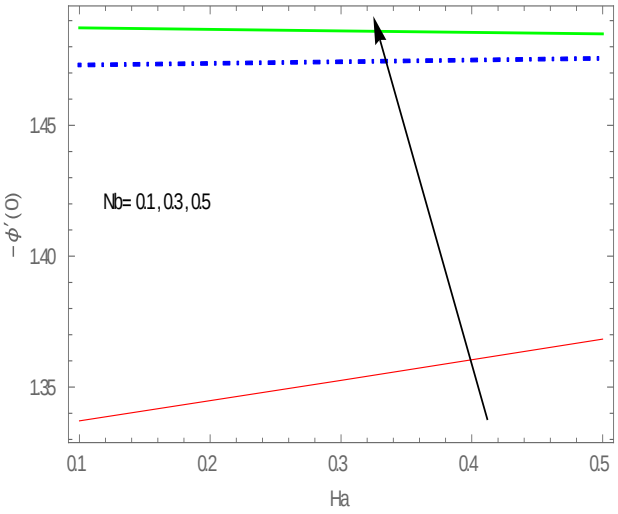

Figure 33. Effect of $N_b\ and\ H_a - \phi'(\eta)$.

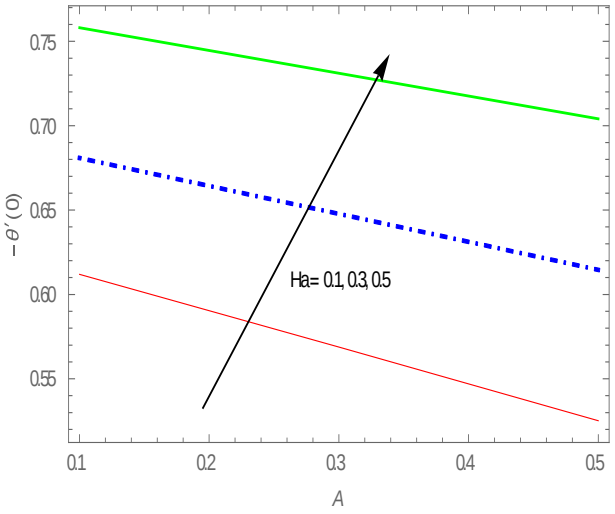

Figure 34. Effect of H_b and $A - \theta'(\eta)$.

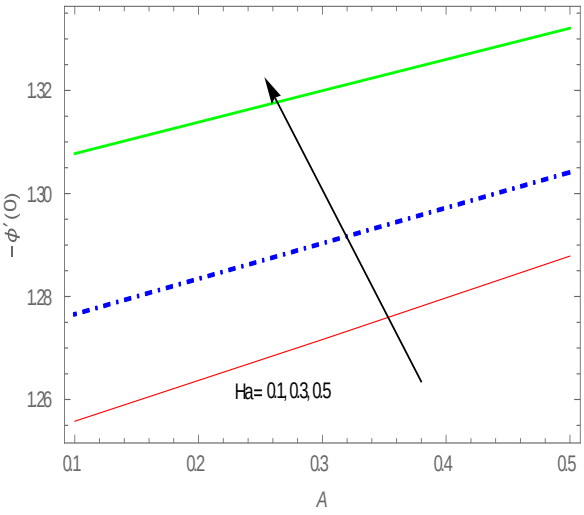

Figure 35: Effect of $H_b\ and\ A - \phi(\eta)$

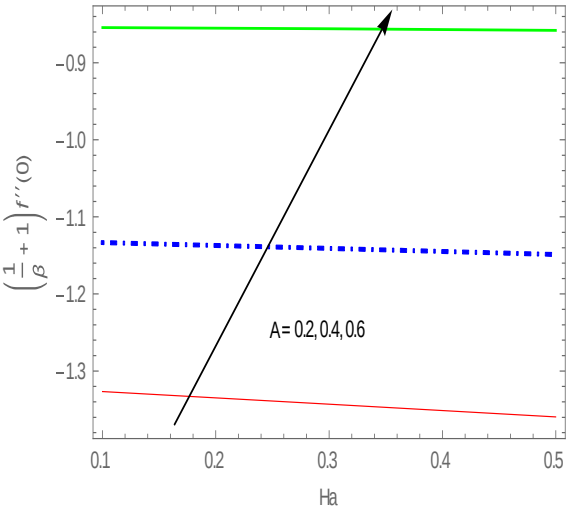

Figure 36: Effect of $A\ and\ H_a\ on\ \left(\frac{1}{\beta}+1\right)f''(0)$

4. Results and Discussion

The numerical solutions are obtained for velocity, temperature, and nanoparticle concentration profiles for various values of physical parameters, such as the slip parameter (λ), the thermal slip parameter (γ), the concentration slip parameter (δ), the thermophoresis parameter (N_t), the Brownian motion (N_b), the chemical reaction parameter (χ), the velocity ratio parameter (A), the heat generation parameter (Q), the Eckert number (Ec), the Casson parameter (β), the Lewis number (Le) and the Hartman number (H_a). The results obtained are presented pictorially in figures 1- 34 for dimensionless velocity, dimensionless temperature, and dimensionless nanoparticle concentration profiles respectively. We compared our result with that of Ahmed and Afify (Haroun et al., 2015) by neglecting the effects of H_a, Q and A. The comparison shows good agreement as presented in Tables 1.

Figures 1-4 displayed the effects of (λ) on the fluid flow, the magnitude of the skin friction coefficient,$f''(\eta)$, the temperature, θ, and the nanoparticle concentration, ϕ profiles. It is observed that an increase in the slip parameter decreases the velocity of the fluid profile and the skin friction coefficient because the high value of the slip parameter corresponds to a reduction in the surface of skin friction while the increase in slip parameter increases both the temperature and nanoparticle concentration profiles. The effects of the thermal slip parameter on the temperature and nanoparticle concentration profiles are depicted in Figures 5 and 6 it is noteworthy that an increase in the thermal slip parameter reduces the thermal boundary layer and nanoparticle concentration distribution. Because heat transfer within the boundary layer fluid reduces with the enhancement of the thermal slip parameter. Figure 7 represents the effects of the concentration profile and it observed that the nanoparticle concentration decrease with an increased concentration slip parameter. A rise in temperature and nanoparticle concentration profiles is noticed in Figures 8 and 9. The impacts of the Brownian motion parameter on heat flow and the nanoparticle concentration distributions are presented graphically in figures 10 and 11. It is observed that the heat flow increase with an increase in the Brownian motion parameter, while the nanoparticle concentration profile decreases.

The dimensionless nanoparticle concentration profiles for various values of $\chi, N_b \; and \; N_t$ are exhibited in figures 12-15 respectively, and the nanoparticle concentration profiles reduce with a rise in chemical reaction for different values of $N_b \; and \; N_t$. Figures 16-23, displayed graphical representative of temperature and nanoparticle concentration distributions for various values of $N_b, N_t \; and \; Le.$ Both the temperature and nanoparticle concentration profiles increase with an increase in $N_b \; and \; N_t$ when Lewis number is 1 or 5 in figures 16 -20, while the reverse is the case in figures 21-23 with the same value of Lewis number. The influence of Eckert number and heat generation parameters on the temperature profiles within the boundary layer region is shown in figures 24 and 25 and it is understood that the temperature profile increased with an increase in the Eckert number. This happened due to viscous heating, the increase in the fluid temperature is enhanced and appreciable for higher values of Eckert number. Physically, Eckert's number relates the kinetic energy to the enthalpy of a fluid, while an increase in heat generation leads to an increase in the temperature throughout the entire boundary layer in figure 25. The heat generation does not only increase the temperature of the fluid but also increases the thermal bounder layer thickness. Figure 26 present the influence of the Casson parameter on the velocity profile and it is worthwhile to note that the velocity profile decreases with an increase in the values of $\beta \; for \; Le = 5 \; and \; P_r = 4.$ From figure 27 and 28, the effects of velocity ratio parameter on the magnitude of the skin friction coefficient and the temperature profiles are presented, it is noticed from figure 27 that the magnitude of the skin friction profile increases with an increase in velocity ratio parameter near the wall, whereas the reverse trend is observed far away from the wall, while the increase in velocity ratio parameter decreased the temperature profile in figure 28. Figure 29 is plotted to see the behavior of Hartman number H_a on the temperature profile and it is seen that temperature profile increases by increasing the value of H_a. Figures 30-31 represent the effect of slip parameter λ and Brownian motion N_b on local Nusselt number$-\theta'(0) \; and \; -\phi'(0)$, while an increase in λ reduces the local Nusselt number and the reverse case is noticed in Sherwood number. Figures 32-33, are depicted to see the behavior of Brownian motion and Hartman number on both $-\theta'(0) \; and \; -\phi'(0)$, and it can be seen from the graphs that there is a decrease in local Nusselt number and an increase in Sherwood number with an increase in the value of the Brownian motion parameter. Effect of Hartman and velocity ratio parameters are depicted in figures 34-35, and both local Nusselt and Sherwood numbers increase with an increase in Hartman number, while figure 36 represents the effect of velocity ratio on the magnitude of the skin friction coefficient and rise in velocity ratio leads to an increase the skin friction coefficient.

5. Conclusions

Two-dimensional flow of stagnation point heat flow and mass transfer in a Casson Nanofluid with thermodiffusion and an inclined magnetic field is considered and the numerical computation is performed via the Spectral Collocation Method. From the study, we analyzed that rise in the thermophoresis parameter enhances both the temperature and

nanoparticle concentration profiles, while the velocity profile decreases with an increase in the Casson parameter. The increase in the magnetic parameter enhances the temperature and nanoparticle concentration profiles.

References

Afify, A. (2017). The influence of slip boundary condition on Casson nanofluid flow over a stretching sheet in the presence of viscous dissipation and chemical reaction. *Mathematical Problems in Engineering*, 2017, 1-12. doi: https://doi.org/10.1155/2017/3804751

Alsedais, N. (2017). Heat Generation and Radiation Effects on MHD Casson Fluid Flow Over a Stretching Surface Through Porous Medium. *European Journal of Advances in Engineering and Technology*, 4(11), 850-857.

Awais, M., Hayat, T., Irum, S., & Alsaedi, A. (2015). Heat Generation/Absorption Effects in a Boundary Layer Stretched Flow of Maxwell Nanofluid: Analytic and Numeric Solutions. *PLOS ONE*, 10(6). doi: https://doi.org/10.1371/journal.pone.0129814

Bhattacharyya, K. & Layek, G. (2010). Chemically Reactive Solute Distribution in Mhd Boundary Layer Flow Over a Permeable Stretching Sheet with Suction or Blowing. *Chemical Engineering Communications*, 197(12), 1527-1540, doi: 10.1080/00986445.2010.485012

Choi, S.U. S. & Eastman J. A. (1995). Enhancing thermal conductivity of fluids with nanoparticles. *Proceedings of the ASME International Mechanical Engineering Congress and Exposition*. 66.

Crane, L. J. (1970). Flow past a stretching plate. *Journal of Applied Mathematics and Physics* (ZAMP) 21, 645–647. doi: https://doi.org/10.1007/BF01587695

Fang, T., Zhang, J., & Yao, S. (2009). Slip MHD viscous flow over a stretching sheet – An exact solution. *Communications in Nonlinear Science and Numerical Simulation*, 14(11), 3731-3737. doi: https://doi.org/10.1016/j.cnsns.2009.02.012

Haroun, N. A.H., Mondal, S., & Sibanda, P. (2015). Unsteady Natural Convective Boundary-layer Flow of MHD Nanofluid over a Stretching Surfaces with Chemical Reaction Using the Spectral Relaxation Method: A Revised Model. *Procedia Engineering*, 127, 18-24. doi: https://doi.org/10.1016/j.proeng.2015.11.317

Kumar, P. S., & Gangadhar, K. (2015). Effect of chemical reaction on slip flow of MHD Casson fluid over a stretching sheet with heat and mass transfer. *Advances in Applied Science Research*, 6(8), 205-223.

Mahapatra, T.R. & Gupta, A.S. (2001). Magnetohydrodynamic stagnation-point flow towards a stretching sheet. *Acta Mechanica*, 152, 191–196. doi: https://doi.org/10.1007/BF01176953

Meraj, M. & Junaid, K. (2015). Model for flow of Casson nanofluid past a non-linearly stretching sheet considering magnetic field effects. *AIP Advances*. 5. doi: 10.1063/1.4927449

Pavlov, K. B. (1974). Magnetohydrodynamic Flow of an Incompressible Viscous Fluid Caused by the Deformation of a Plane Surface. *Magnitnaya Gidrodinamika*, 10(4), 146-147.

Reddy C, S., Naikoti, K., & Rashidi, M. M. (2017). MHD flow and heat transfer characteristics of Williamson nanofluid over a stretching sheet with variable thickness and variable thermal conductivity. *Transactions of A. Razmadze Mathematical Institute*, 171(2), 195—211. doi: https://doi.org/10.1016/j.trmi.2017.02.004

Reddy, J.V. R., Sugunamma, V., Sandeep, N., & Sulochana, C. (2016). Influence of chemical reaction, radiation and rotation on MHD nanofluid flow past a permeable flat plate in porous medium. *Journal of the Nigerian Mathematical Society*, 35(1), 48-65. doi: https://doi.org/10.1016/j.jnnms.2015.08.004

Shen, J., Tang, T., & Wang, L-L. (2011). *Spectral Methods: Algorithms, Analysis, and Applications*. Berlin, Heidelberg: Springer. doi: https://doi.org/10.1007/978-3-540-71041-7

Sun, Y-S., Ma, J., & Li, B-W. (2012). Chebyshev Collocation Spectral Method for Three-Dimensional Transient Coupled Radiative–Conductive Heat Transfer. *Journal of Heat Transfer*, 134(9). doi: https://doi.org/10.1115/1.4006596

Zaimi, K. & Ishak, A. (2016). Stagnation-Point Flow towards a Stretching Vertical Sheet with Slip Effects. *Mathematics*, 4(2), 27. doi: https://doi.org/10.3390/math4020027

Rao, M. E.& Sreenadh, S. (2017). MHD Flow of a Casson Fluid over an Exponentially Inclined Permeable Stretching Surface with Thermal Radiation, Viscous Dissipation and Chemical Reaction. *Global Journal of Pure and Applied Mathematics*, 13(10), 7529-7548.

Ishak, A., Jafar, K., Nazar, R., & Pop, I. (2009). MHD stagnation point flow towards a stretching sheet. *Physica A: Statistical Mechanics and its Applications*, 388(17), 3377-3383.